CORROSION SCIENCE AND TECHNOLOGY, Vol.23, No.2(2024), pp.104~112 pISSN 1598-6462 / eISSN 2288-6524
[Research Paper] DOI: https://doi.org/10.14773/cst.2024.23.2.104

Characterization of Solidification and Microstructure of an Al-Zn-Mg-Si Alloy

He Tian[1,†], Dongdong Qu[1], Zherui Tong[1], Nega Setargew[2], Daniel J. Parker[2], David StJohn[1], and Kazuhiro Nogita[1]

[1] *School of Mechanical and Mining Engineering, The University of Queensland, Brisbane Qld 4072, Australia*
[2] *BlueScope Innovation Lab, Port Kembla, NSW 2505, Australia*

(Received January 11, 2024; Revised March 04, 2024; Accepted March 05, 2024)

Al-Zn-Mg-Si alloy coatings have been developed to inhibit corrosion of cold rolled steel sheets, and an understanding of the alloy system helps prevent coating defects. We used a Bridgman furnace to characterise the nature and formation mechanisms of the phases present in the quaternary system with 0.4 wt% Fe. In the directional solidification experiments we imposed steep temperature gradients and varied the pull rate. After the samples were quenched in the furnace, detailed characterization of the samples was carried out by electron microscopy (SEM/EDS). From the dT/dt vs T plots of the cooling curves of the alloys, the solidification path was determined to be Liquid$\xrightarrow{544\text{-}558}$α-Al$\xrightarrow{453\text{-}459}$Al/$Mg_2Si$$\xrightarrow{371\text{-}374}Al/Zn\xrightarrow{331\text{-}333}$Zn/$mgZn_2$. The formation mechanisms of the Mg and Zn containing phases and their morphology was discussed together with the effects of the cooling rate. Key findings include the lengthening of the mushy zone in directionally solidified samples remelted against a positive temperature gradient, as well as an enrichening of the α-Al phase by Zn through remelting. Mg_2Si and other Si based phases were observed to adopt a much finer faceted microstructure in favour of a script-like microstructure when exposed to the higher cooling rate of coolant quenching.

Keywords: *Directional, Solidification, Al-Zn, Bridgman, SEM*

1. Introduction

Al-Zn-Mg-Si alloys, denoted 'AM', have been developed to be used as a corrosion inhibitive coating on cold rolled steel sheets as a durable alternative to Zn-based coatings, and offer both galvanic and barrier protection against corrosion of the substrate steel sheet [1]. This coating can be used in conjunction with additional primer and paint layers, but proper adhesion of the base layer is crucial for optimal coating performance. Compared to traditional Al-Zn based coatings, Al-Zn-Mg-Si coatings provide improved corrosion resistance and durability through the presence of the $MgZn_2$ and Mg_2Si phases, with the former providing galvanic/cut resistance and the latter acting as a barrier in corrosion pathways [2].

In light of defects observed on the production line, to maximise the quality of this coating it is important to understand the solidification sequence of this alloy system, and therefore the formation mechanisms of its phases. Work has been done previously to characterise this system through thermal analysis and bulk solidification [3], but due to the complex quaternary nature of the system more advanced methods are desired. It was proposed that this system be studied using a Bridgman furnace, which is often used for directional solidification or directional melting [4]. The Bridgman furnace is valuable in the fact that it can be used to present a solidified microstructure quenched at a continuous range of temperatures. This is achieved by holding the sample in the temperature range of interest, allowing the alloy to melt then rapidly quenching in the coolant bath held beneath the furnace. Observation of this quenched microstructure will allow deconvolution of the solidification sequence.

Previous work has been done by Tong *et al.* [3] to characterise the alloy system from a combination of analysing the cooling curves and SEM/EDS microscopy.

The goal of the directional solidification experiments will be to verify Tong *et al.'s* [3] findings and to study the mechanisms proposed in greater detail.

†Corresponding author: he.tian@uq.net.au

2. Method and Materials

2.1 Sample preparation

Ingots of Al-Zn-Mg-Si were heated in a resistance furnace to 750 ºC inside a boron nitride coated clay crucible and held for 120 min to allow the alloy to homogenise. The alloy was then quickly cast into a three-pronged graphite pencil mould pre-heated at 180 ºC, which was allowed to air cool on the bench for 10 min before being removed from the mould.

The cast cylinders were cut from their sprue and turned on a lathe to a nominal outer diameter of 4.5 mm, these cylinders were then coated in boron nitride solution and inserted into a stainless steel tube of 4.6 mm inner diameter, which was likewise internally coated with boron nitride inside to prevent reaction between the alloy and the tube. This tube complete with the sample was taken and attached to the frame of the Bridgman furnace, with the alloy segment positioned inside the furnace. The temperature gradient inside of the furnace was first measured by running a type N thermocouple encased inside a stainless steel tube identical to that used for the sample itself.

The furnace used for these experiments maintains a temperature gradient through the combined use of its heating element and constantly circulating ethylene glycol coolant, with the latter also used to quench the samples upon completion of the experiment. The rate at which the sample moved through the furnace was controlled via a gear driven controller and the sample was pulled parallel to the direction of heat flow.

2.2 Directional melting

The furnace was moved downwards at a steady rate of 0.02 mm/min for 200 min, to encourage crystal growth and mitigate the sedimentation of impurities and heavier phases within the alloy. Upon completion of the pull, the furnace was immediately stopped, and the sample released from the frame, allowing it to be rapidly quenched in a tube of refrigerated and recirculating ethylene glycol coolant held at approximately 4 ºC. The quenched tube would be removed from the coolant, the sample removed from inside, cut into four individual segments labelled ‘1’, 2’, ‘3’ and ‘4’ in ascending temperature range, longitudinally sectioned, mounted in Struers Polyfast conductive resin and polished for electron microscopy using silicone carbide paper and diamond solution.

During directional melting the sample began at 25 mm from the bottom of the furnace, and was pulled for a distance of 4 mm. The sample was 100 mm long in total to allow for temperature variations at either end of the furnace. The target temperature zone was between 200 ± 20 ºC and 600 ± 20 ºC. Directional melting has been chosen as the method for identifying phase transformation temperatures as the system is closer to being at steady state, as there is minimal remelting. The

Table 1. List of samples and experiments for directional solidification and melting of 0.4 wt% Fe AM

Sample name	Experiment type	Pull rate	Pull length	15 mm temp (ºC)	40 mm temp (ºC)	65 mm temp (ºC)	90 mm temp (ºC)	105 mm temp (ºC)
A	Directional melting	0.02 mm/min	4 mm	208.24	392.12	541.23	639.55	696.50
B	Directional melting	0.02 mm/min	4 mm	202.90	382.98	525.35	622.06	679.63
C	Directional melting	0.02 mm/min	4 mm	194.53	398.48	538.80	631.60	685.70
D	Directional solidification	0.5 mm/min	60 mm	149.25	344.32	495.15	604.03	647.64
E	Directional solidification	0.5 mm/min	60 mm	149.25	344.32	495.15	604.03	647.64
F	Directional solidification	0.5 mm/min	60 mm	183.11	375.33	518.28	615.72	655.00
G	Directional solidification	0.25 mm/min	60 mm	183.11	375.33	518.28	615.72	655.00
H	Directional solidification	0.25 mm/min	60 mm	159.67	370.90	514.96	614.87	655.56
I	Directional solidification	0.25 mm/min	60 mm	164.31	369.27	537.10	578.90	653.69
J	Directional solidification	0.1 mm/min	60 mm	145.94	372.38	464.52	582.05	656.32
K	Directional solidification	0.1 mm/min	60 mm	145.51	354.64	503.83	609.20	651.69
L	Directional solidification	0.1 mm/min	60 mm	145.51	354.64	503.83	609.20	651.69

small pull rate is used to encourage crystal growth along the direction of pull.

2.3 Directional solidification

The directionally solidified samples were prepared in an identical fashion, but using a different stopper they were positioned higher than the directionally melted samples. This would mean each part of the sample would pass through the highest temperature zone of the furnace before being resolidified. These samples were pulled at rates of 0.5 mm/min, 0.25 mm/min and 0.1 mm/min with three repeats for each speed. Directionally solidified samples were segmented, mounted and processed by an identical procedure to that of directionally melted samples.

During directional solidification the sample began at 75 mm from the bottom of the furnace, and was pulled for a total distance of 60 mm. The sample was 100 mm long in total to allow for temperature variations at either end of the furnace. The target temperature zone was between $200 \pm 20\ ^{o}C$ and $600 \pm 20\ ^{o}C$. Directional solidification was used to study the effect of growth rate on the sample, as the variable pull speed was used to alter the G/V ratio, where G is the temperature gradient and V is the pull rate. The list of samples is presented in Table 1.

3. Results and Discussion

3.1 Variation of pull rate

Previous experiments have shown that by decreasing the pull rate, a corresponding increase in the length of the mushy zone may be observed. Measurements were taken of the primary α-Al dendrites found at the liquid-solid interface for samples pulled at the three different speeds, and measurements for the dendrite arm spacing (DAS) taken at both the liquid-solid boundary as well as in the solidified microstructure. The G/V ratios were calculated to be 3.42×10^{9}, 1.37×10^{9}, and $6.84 \times 10^{8} \frac{K_s}{m^2}$.

Measurements were taken in the same temperature zone for each sample (area '4') for consistency, both in the initial α-Al growth and in the subsequent heterogeneously nucleated dendrites in the interdendritic area. Measurement of DAS across fifteen different points for each pull rate found that with increasing pull rate, the DAS would decrease accordingly. Measurement of the mushy zone liquid/solid boundary also found that the length of the mushy zone decreased with increasing pull rate. The average DAS measured across 0.1 mm/min, 0.25 mm/min and 0.5 mm/min was found to be 75.83, 60.52 and 58.62 μm resulting in a downward trend in DAS. This suggests that the pull rate in this directional solidification experiment was proportional to the growth rate of the alloy system, with higher growth rates exhibiting finer microstructure. A uniform, fine, dendritic microstructure is desirable for coatings as a network of α phase with interdendritic Mg and Zn phases provides a corrosion resistant network structure [1].

It was found that the reduction in DAS was less noticeable between the 0.25 mm/min sample and the 0.5 mm/min sample than between the 0.1 mm/min and 0.25 mm/min sample. It is believed that the threshold G/V ratio for the transition from cellular dendritic to columnar dendritic is found between the 0.1 mm/min and 0.25 mm/min pull rates. The microstructure seen in Fig. 1a shows fewer signs of branching with growth mostly restricted to the primary dendrite arms.

3.2 Microstructural phase identification using directional melting inside a bridgman furnace

SEM images of the directionally solidified samples show that from the liquid, the first phase to nucleate are the α-Al dendrites, which grow in a finger-like formation and trap pockets of interdendritic Zn rich liquid. The goal of the directional melting experiment is to capture the formation temperatures and microstructures of the alloy system with respect to existing thermal analysis and simulation data.

3.3 α-Al phase

The α-Al phase largely dominates the volume fraction of the sample composition, hence to study the formation of further phases, special attention is paid to the interdendritic liquid region in-between them. High magnification micrographs of the interdendritic region during solidification in Fig. 1. Microstructure and composition of the interdendritic area over 18 mm in a directionally melted AM sample. Images a-l are in taken with increasing temperature, with 'a' taken in the initial stages of α solidification and 'l' taken in the final stage show that small dendrites of α phase form from the Al-Zn eutectic region and are absorbed into large α-Al

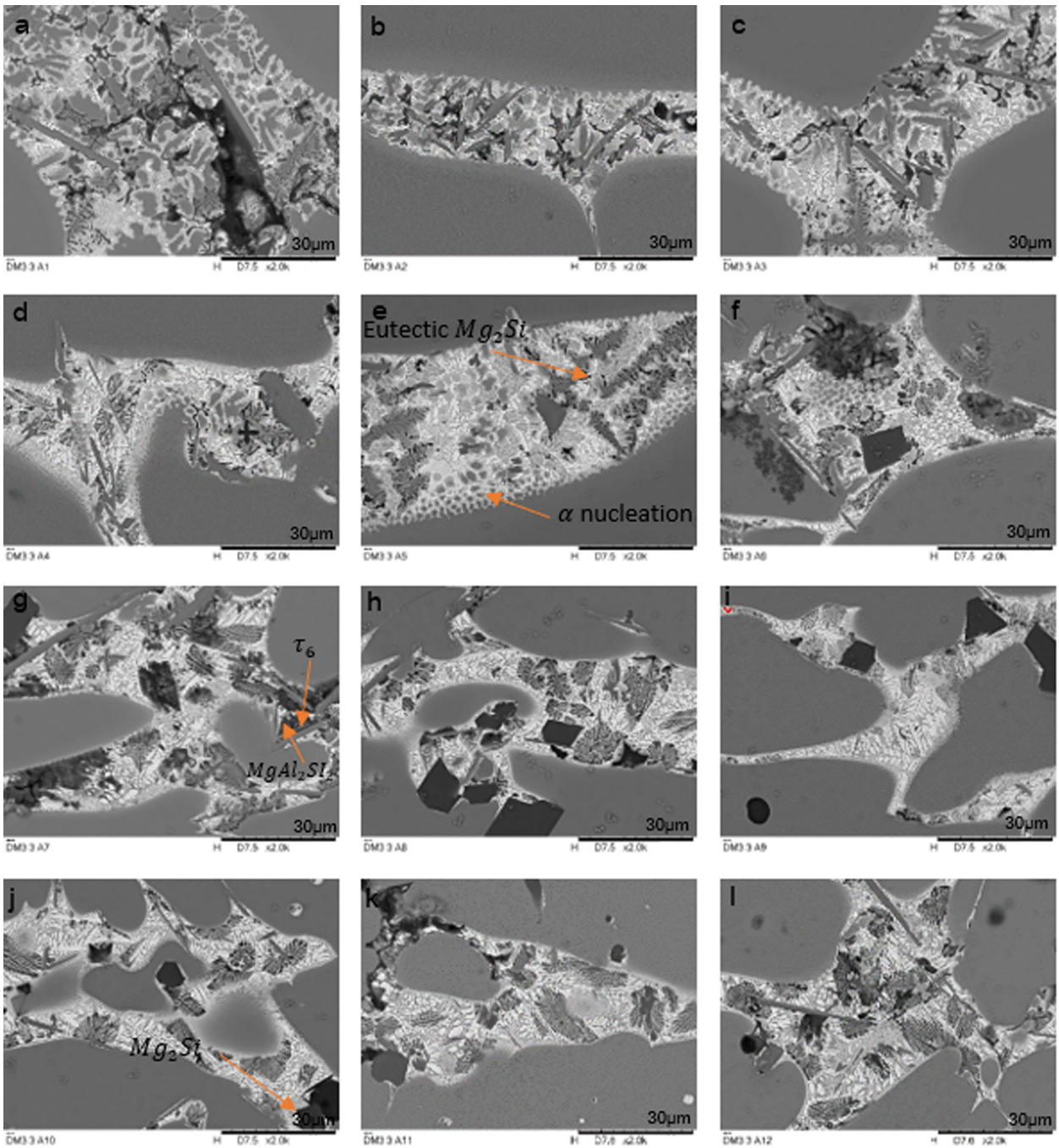

Fig. 1. Microstructure and composition of the interdendritic area over 18 mm in a directionally melted AM sample. Images a-l are in taken with increasing temperature, with 'a' taken in the initial stages of α solidification and 'l' taken in the final stage

crystals. The α-Al phase nucleates heterogeneously from the melt with high Zn content and rejects this Zn back into the interdendritic liquid to form a region rich in Mg and Zn. The formation of small α-Al dendrites under 10 μm observed in the melt is believed to come from the rapid solidification of remaining Al suspended in the melt during the rapid quench. A positive Zn gradient may be observed along the borders of each of the Al dendrites, representing the rejection of Zn as the α phase continues to solidify.

Travelling downwards along the temperature range, the α phase continues to grow until the Al content of the interdendritic fluid has been exhausted, and the microstructure consists of a network of α phase and divorced Mg/Zn eutectics.

3.4 τ_6 and τ_{5c} phases

The τ_6 and τ_{5c} phases are Fe based intermetallic phases that form early in the solidification sequence, at a similar point to α-Al. The τ_6 phase has been known to act as a heterogeneous nucleating point for $MgAl_2Si_2$ and takes on a needle-like morphology whereas the τ_{5c} phase is observed with a faceted cubic morphology. A τ_6 needle being used as a heterogeneous nucleation site for $MgAl_2Si_2$ can be seen in Fig. 1g. This shows the τ_6 phase in the quenched liquid phase alongside Mg_2Si, the presence of τ_6 needles cutting across α dendrites suggests that the formation of this phase precedes that of the α-Al phase.

3.5 Mg phases

The Mg_2Si phase is known to be vital in the barrier protection performance of the alloy. According to prior thermodynamic studies by Tong *et al.* [3], the Mg_2Si phase does not form until approximately 460 ºC, therefore it is unusual to identify it within the interdendritic liquid while the α-Al phase is still in the early stages of solidification. It is believed that these small growths of Mg_2Si, usually between 10 μm and 30 μm in length, are a result of growth in the liquid during quenching. Their microstructure bears a distinct, fine fishbone morphology and is most typically seen as forming a eutectic with α-Al. In the lower temperature regions of the sample, Mg_2Si dendrites formed inside of the furnace feature a coarser divorced morphology as seen in Fig. 1j. These Mg_2Si dendrites typically range from 10 μm to 100 μm, and it is believed that the greater size of these dendrites is due to an increased availability of Mg rejected from the α phase as well as grain coarsening induced by the slower cooling of the alloy, resulting in high temperature annealing.

Fig. 1 shows the progression of the interdendritic microstructure in twelve 90 μm increments from the high temperature α-Al/liquid mushy zone to the almost fully solidified microstructure. From 1(f) onwards it can be observed that the Al content is no longer high enough for the homogeneous nucleation of α-Al phase, however the Al may still be seen to form clusters of eutectic Mg_2Si phase whose growth most likely appeared during the quench. From 1(f) onwards, the formation of faceted Si crystals can also be identified. The positioning of these crystals relative to the surrounding α phase suggests that the Si phase nucleation occurs during the α-phase solidification process.

However, the Mg_2Si phase was only observed in one of the three directional melting samples in the expected range in its divorced form. In its place faceted Si was observed instead which was confirmed through EDS in Fig. 3. This was predicted by the experimental phase diagram generated using Thermo Calc 2021a (aluminium library) (Fig. 2), which approximated its formation

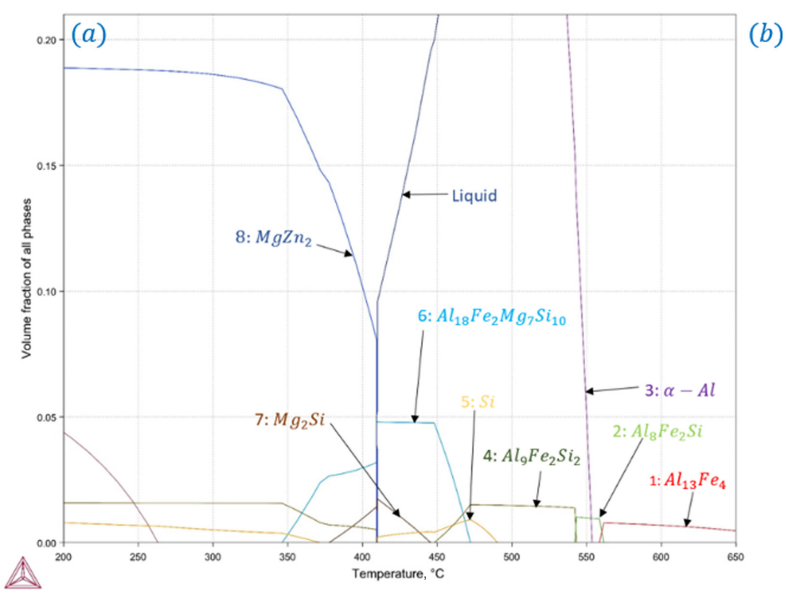

(b)

Temperature (°C)	Reactions in AM-0.4Fe
700	Liquid AM → $FeAl_3$
561	Liquid AM + $FeAl_3$ → τ_{5c}
553	Liquid AM → α − Al
543	τ_5 → τ_6
490	Liquid AM → Al/Si
471	Liquid AM + τ_6 + Si → $Al_{18}Fe_2Mg_7Si_{10}$
444	Liquid AM + Si → Al/Mg_2Si
410	Liquid AM + Mg_2Si + Si → $Al/MgZn_2$ + Liquid AM (Si)
409.5-410.1	Liquid AM + Mg_2Si → $Al/MgZn_2$ + Liquid AM (Si)
409.5	Liquid AM + $Al_{18}Fe_2Mg_7Si_{10}$ → $Al/MgZn_2$ + Mg_2Si + τ_6
378-409.5	α − Al + Mg_2Si + Al18Fe2Mg7Si10 → $MgZn_2$ + T6
378	α − Al + $Al_{18}Fe_2Mg_7Si_{10}$ → $MgZn_2$ + τ_6
372.3	α − Al + $Al_{18}Fe_2Mg_7Si_{10}$ → $MgZn_2$ + τ_6 + Si
345	α − Al → $MgZn_2$ + Si
263	α − Al → Zn

Fig. 2. (a) Thermo Calc 2021a (aluminium library) one-axis equivalent phase diagram for 0.4 wt% Fe AM alloy, (b) tabulated summary of theoretical phase transformations from the Thermo Calc phase diagram

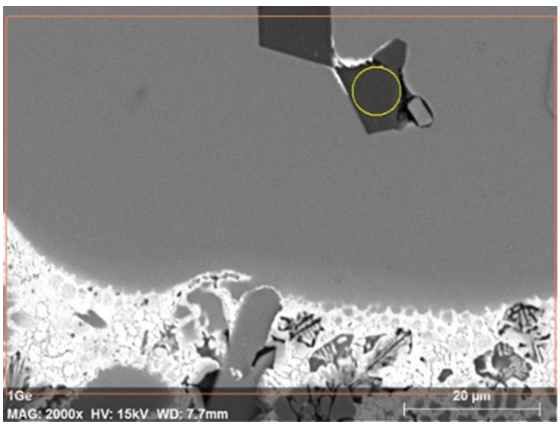

Spectrum: Point

Element	AN	Series	unn. C [wt.%]	norm. C [wt.%]	Atom. C [at.%]
Silicon	14	K-series	81.80	79.79	83.85
Aluminium	13	K-series	10.49	10.23	11.19
Zinc	30	K-series	9.62	9.38	4.24
Magnesium	12	K-series	0.61	0.60	0.73
Iron	26	K-series	0.00	0.00	0.00
		Total:	102.52	100.00	100.00

Fig. 3. Si phase nucleation following solidification of α phase

temperature as 490 ºC. The one axis equivalent phase diagram represents the theoretical equilibrium molar fraction of each phase at constant composition as temperature is varied. The phase diagram was calculated for 0.4 wt% Fe as due to continuous deposition of Fe from the steel sheet in the hot dip process, this has been found to be the equilibrium concentration in a typical factory setting [5].

3.6 Zn-based phases

To verify the degree of Zn rejection into the liquid, EDS spot scans were taken at three points along the α-Al phase gradient leading to the boundary of the dendrite in a directionally solidified sample in Fig. 4. A clear positive trend was found for the concentration of Zn as distance to the border of the sample decreased, along with an accompanying decrease in the levels of Al, which at the boundary is approximately 70 % of the value measured in the core of the dendrite, showing consistency with the Al-Zn phase diagram [6]. The Mg content of the α phase dendrite also decreased with increasing proximity to the edge of the dendrite.

The migration of Zn into the interdendritic area leads to the formation of an Al-Zn eutectic, which initially appears as a halo surrounding α phase dendrites as seen in Fig. 5. Diffusion of Mg and Zn react to form $MgZn_2$ and elemental Zn, which serve an important role as sacrificial protection in the AM coating [1]. It was observed that in the Zn-Mg phase diagram, as Mg availability in the interdendritic liquid decreases, pure Zn

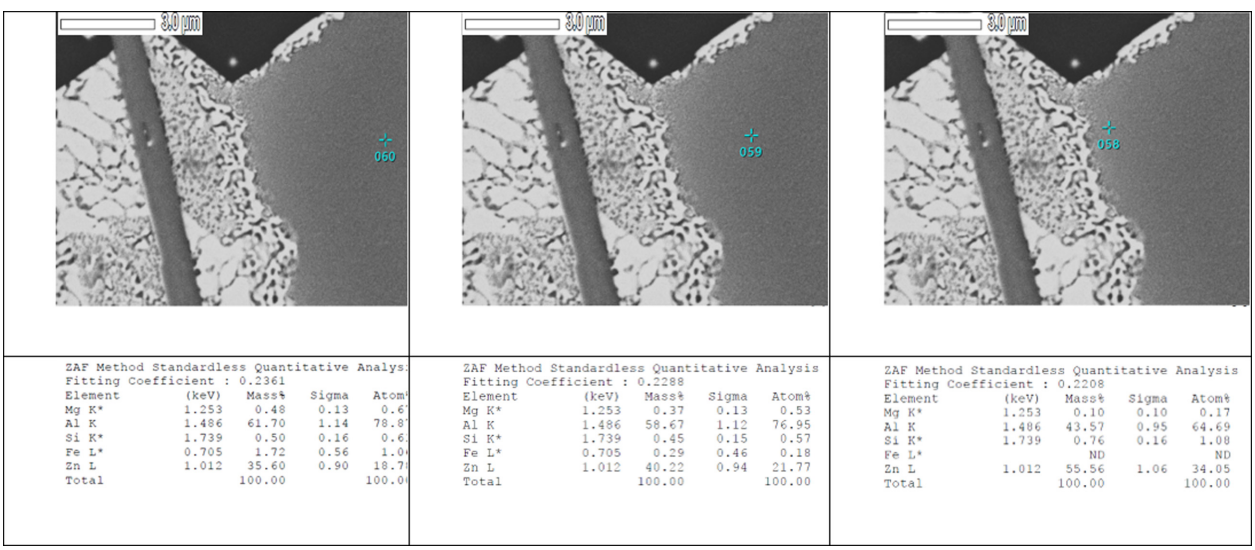

Fig. 4. EDS analysis of Zn content in α phase dendrite

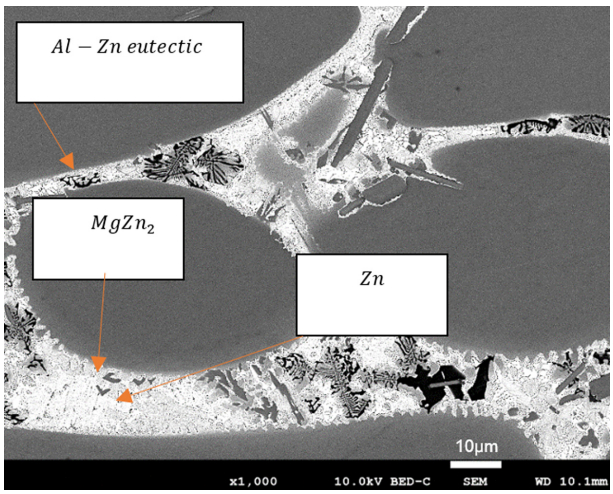

Fig. 5. DM3 part 3 interdendritic microstructure

begins to form preferentially to $MgZn_2$, leading to a higher likelihood of Zn formation surrounding Mg_2Si crystals.

4. Confirmation of Internal Sample Temperature Gradient and Measured Temperature Gradient

To verify the phase transformation temperatures, the microstructure of the directionally solidified samples must be compared to the thermocouple temperature measurement. This was done by identifying points of major phase transformation in the microstructure, measuring the distance between them and corresponding these to phase transformation temperatures identified through Tong *et al.*'s [3] cooling curve experiments.

These values were verified by observing the continuous microstructure in the directionally solidified samples and applying a temperature scale alongside a distance scale. The temperature gradient inside the furnace was measured and was known for each pull test, however its correspondence to the temperature gradient presenting inside of the sample must be confirmed. The formation of the α-Al phase was used to verify the temperature gradient due to its high prominence in the microstructure, as seen in Fig. 6.

The thermocouple measured temperature gradients for directional melt 1 (sample A), directional melt 2 (sample B) and directional melt 3 (sample C) were 5.7 K/mm, 5.7 K/mm and 5.8 K/mm. Measurement of the volume fraction of α-Al phase was performed using Image J thres hold analysis across 1000 μm sections of a back scattered

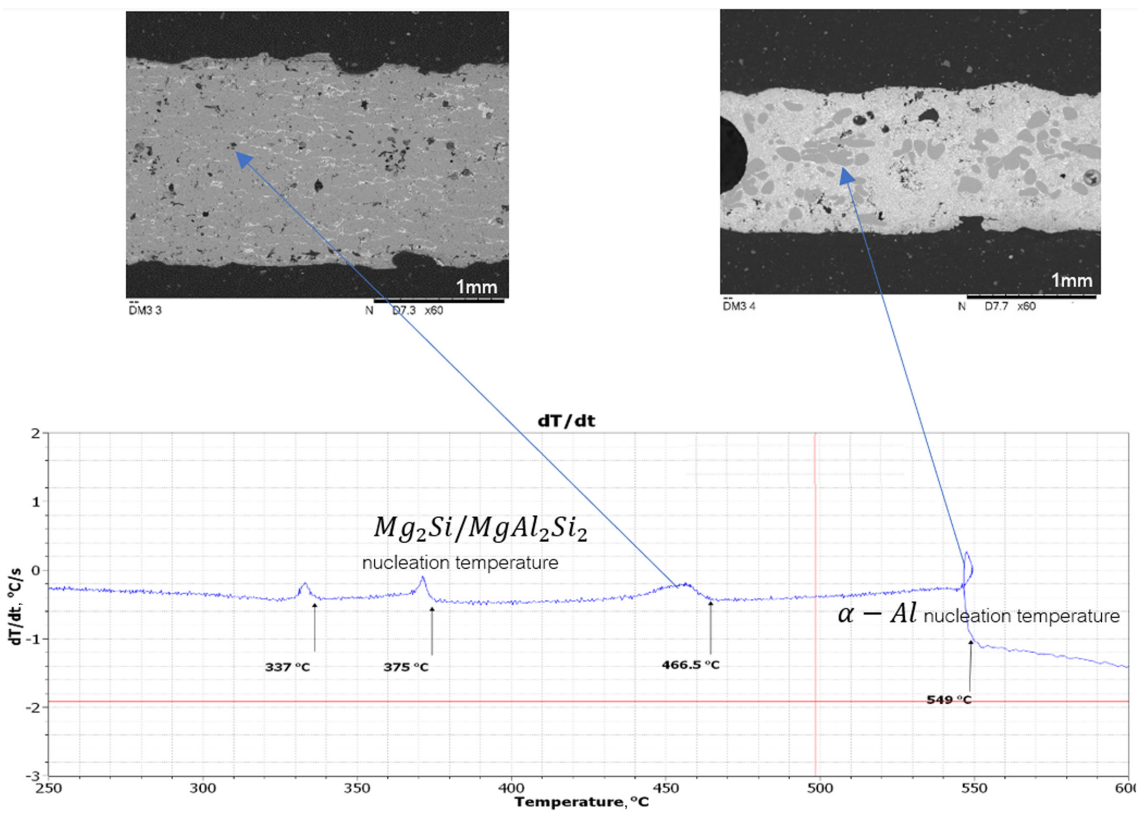

Fig. 6. Comparison of alloy microstructure to cooling curve

Table 2. Calculated thermal gradient comparison to experimental temperature gradient for directional melting experiments

Experiment number	Measured thermocouple temperature gradient (K/mm)	Measured α-Al solidification distance (mm)	Experimental temperature gradient (K/mm)
M	5.68	27	4.78
N	5.69	20	6.45
O	5.80	23	5.60

composite image taken using a Hitachi TM3030 SEM at 15 keV. The data was processed and the point at which the α-Al content plateaued was considered the end of the α phase transformation, which should immediately be followed by the second solidification peak corresponding the $Mg_2Si/MgAl_2Si_2$ phase transformation. When occurring during natural solidification these phases adopted a divorced microstructure unlike the eutectic microstructure observed inside the cooled liquid.

Originally the temperature difference taken to calculate the gradient across the sample was the difference in initiation and completion temperature (T_I and T_C) for the α phase, which was known to be 6.5 K from the thermal curve analysis, which would result in a temperature gradient of 0.24 K/mm to 0.33 K/mm, well below the predicted temperature gradient of 5.7 K/mm to 5.8 K/mm. The original assumption that the two points highlighted in Fig. 6. Comparison of alloy microstructure to cooling curve corresponded to the initial peak for α phase solidification was incorrect. However, with confirmation in Fig. 3 that the dark faceted phase which appeared at the lower temperature highlight was Si. With reference to the one axis equivalent phase diagram in the nucleation temperature for Si can be estimated to be 420 ºC. This phase transformation was not clearly observed in the thermal analysis, but this may be attributed to Si's low heat of fusion of approximately 50 kJ/mol [7]. Taking the difference between the T_I of the α phase and Si, the approximate temperature gradients in the samples can be calculated and are tabulated in Table 2.

The calculated values of thermal gradient were found to fall within the experimental error of the measurements taken, hence the thermal gradient measured by thermocouple may be tentatively applied to identify the nucleation temperatures of each phase, using the nucleation temperature of α-Al as a reference. The reason that the temperature against distance measurement from the furnace calibration graphs was not used directly was to mitigate measurement errors during experimental setup. Hence, the average nucleation temperatures across the three directional melting experiments for the phases as measured using the experimental thermal gradient are presented in Table 3.

Table 3. Measured nucleation temperatures for phases

Phase	Measured initiation temperature (T_I)	Measured completion temperature (T_0)
α-Al	558 ºC	544 ºC
$Mg_2Si/MgASi_2$	459 ºC	453 ºC
Al-Zn	374 ºC	371 ºC
$MgZn_2$	333 ºC	331 ºC

Factors which may contribute to the inconsistency in thermal gradient may include measurement inaccuracies in the thermocouple used to record the furnace temperature profile, non-steady state solidification and non-uniform heat flux inside of the furnace. None of these are believed to be significant enough to cause the magnitude of the error, Hubert *et al.* [8] only observed a 3 mm discrepancy in the location of the liquid-solid front as a result of heat flux effects at the thermocouple tip. Non-steady state solidification has been considered as the ratio of temperature gradient to growth rate has resulted in a dendritic microstructure as opposed to columnar or planar structures more often seen with higher G/V ratios [9]. The heat transfer from the tube to the coolant was considered to have a negligible effect on the solidification process due to the relative specific heat and mass of the ethylene glycol mixture compared to that of the sample tube.

5. Conclusions

Directional solidification and directional melting experiments were conducted on a 0.4 wt% Fe Al-Zn alloy used for coating steels to better understand the solidification sequence and the factors affecting the final

microstructure. α phase was observed to nucleate first alongside the Fe based τ_6 and τ_{5c} phases, followed by Si and $Mg_2Si/MgAl_2Si_2$ and lastly as Zn is rejected outwards from the α phase, Al-Zn eutectics and $MgZn_2$ form. Directional solidification at three different rates was used to identify the effect of growth rate on microstructure, and it was found that the transition G/V ratio for cellular dendritic and columnar dendritic lied between the 0.1 mm/min and 0.25 mm/min pull rates. Measurement of the solidified microstructure from the directional melting experiments was performed to verify the measured temperature gradient in the alloy, and using this the nucleation temperatures of the primary phases were confirmed experimentally. Further work is recommended for verification of the temperature gradient inside the sample against thermocouple measurements.

References

1. BlueScope, Activate Technology [Article] [cited 2022 26/03/2022] (2022). [page error] http://www.steel.com.au/articles/article-46-activate-technology
2. BlueScope Steel Limited, Development of aluminium/zinc/magnesium alloycoating for next generation ZINCALUME® steel with Activate® technology, *Technical Bulletin*, Revision 6 (2022). https://cdn.dcs.bluescope.com.au/download/ctb-06
3. Z. Tong, Master's Thesis, pp. 3 - 12, The University of Queensland, Brisbane (2022).
4. D. C. Stockbarger, The Production of Large Single Crystals of Lithium Fluoride, *Review of Scientific Instruments*, **7**, 133 (1936). Doi: https://doi.org/10.1063/1.1752094
5. N. Setargew, J. Hodges, and D. Parker, Dross Intermetallic Compound Formation and the Alloy Layer in 55%Al-Zn Coating Systems, pp. 1 – 30, Steel Research Hub, University of Wollongong, Australia (2015).
6. A. Pola, M. Tocci, and F. E. Goodwin, Review of microstructures and properties of zinc alloys, *Metals*, **10**, 253 (2020). Doi: https://doi.org/10.3390/met10020253
7. P. W. Atkins and L. Jones, *Chemical principles : the quest for insight*, *2nd ed.*, W. H. Freeman, Highlighting, New York (2002).
8. J. A. Hubert, A. L. Fripp, and C. S. Welch, Resolution of the discrepancy between temperature indicated interface and radiographically determined interface in a vertical Bridgman furnace, *Journal of Crystal Growth*, **131**, 75 (1993). Doi: https://doi.org/10.1016/0022-0248(93)90398-G
9. D. M. Stefanescu, *Science and Engineering of Casting Solidification, 2nd ed.*, p. 252, Springer US, New York (2009).